PHYSICAL REVIEW B **71**, 041305(R) (2005)

Phonon Bloch oscillations in acoustic-cavity structures

N. D. Lanzillotti Kimura,[1] A. Fainstein,[1] and B. Jusserand[2]
[1]*Centro Atómico Bariloche & Instituto Balseiro, C.N.E.A., 8400 San Carlos de Bariloche, Río Negro, Argentina*
[2]*Laboratoire de Photonique et de Nanostructures, CNRS, Route de Nozay, 91460 Marcoussis, France*
(Received 14 October 2004; published 21 January 2005)

We describe a semiconductor multilayer structure based in acoustic-phonon cavities and achievable with molecular beam epitaxy technology, designed to display acoustic-phonon Bloch oscillations. We show that forward and backscattering Raman spectra give a direct measure of the created phononic Wannier-Stark ladder. We also discuss the use of femtosecond laser impulsions for the generation and direct probe of the induced phonon Bloch oscillations. We propose a gedanken experiment based in an integrated phonon source-structure-detector device, and we present calculations of pump and probe time-dependent optical reflectivity that evidence temporal beatings in agreement with the Wannier-Stark ladder energy splitting.

DOI: 10.1103/PhysRevB.71.041305 PACS number(s): 68.60.Bs, 78.67.Pt, 78.30.Fs, 63.22.+m

Electronic Bloch oscillations, i.e., oscillations of an electron induced by a constant electric field in the presence of a periodic potential,[1] are a beautiful and clear example of quantum effects in solids. When an electric field is applied on a charged particle in a crystal, its wave vector increases with time. Thereafter, Bragg interference leads to a velocity reduction, and finally to a sign change at the band edge. Notwithstanding its simplicity, for many years the issue was controversial and only quite recently the existence of electronic Bloch oscillations has been definitively established. In normal crystals the large Brillouin zone and electron relaxation lead to an overdamped behavior characterized by Ohm's law. Instead, electronic Bloch oscillations are observable in semiconductor superlattices (SL's) due to the Brillouin zone reduction.[2]

Motivated by the concepts introduced for electrons in crystals, Bloch oscillations of atoms in an accelerating standing wave of light have been reported.[3] On the other hand, recently *photon* Bloch oscillation devices based in optical microcavities have been proposed,[4] and related reflectivity and time-resolved optical transmission features have been observed in structures grown on porous silicon.[5] The concept behind these devices is also quite nice and simple. The optical microcavities provide the discrete photonic states which can couple through photon mirrors thus leading to photonic minibands. The spatial dependent energy gradient, equivalent to the electric field for electrons, can be achieved, e.g., by varying the refractive index.[5] As compared to electrons, photon dephasing mechanisms are less effective and thus Bloch oscillations are, in principle, more easy to observe. On the other hand, photonic minibands require a large number of optical microcavities (around 30–50), amounting to total thicknesses larger than $40-50\ \mu$m.[4] This is too large for current molecular beam epitaxy (MBE) semiconductor technology. For this reason the reported structures were grown using electrochemical methods of porous silicon nanostructuring that do not have this limitation.[5] The drawback is that the quality of the samples is not as good, layer interfaces and refractive indices are not that well controlled, and optical residual absorption becomes an important issue in the performance of the structures.

Sound in solid media is also described by a wave equation, the relevant parameters being the material density and sound velocity, and the boundary conditions establishing the connection between displacement and strain between two different materials. Thus, the above concepts applied to electrons and photons can be extended to phononic structures. In fact, Stark-ladder resonances in the phonon spectra of piezoelectric composites have been recently reported.[6] In this communication we propose semiconductor multilayer structures capable of displaying *acoustic-phonon* dynamics similar to Bloch oscillations. The building block of the structures are acoustic-phonon cavities as recently introduced by Trigo and co-workers.[7] The phonon wavelength is only a few nanometers (phonon frequencies being in the THz range), and thus the sample full size and required interface layer quality are achievable with actual MBE technology. In addition, acoustic-phonon mean-free paths are large[8] compared to the structure size (typically below a micron) and thus dephasing is not a critical issue. We present calculations of phonon reflectivity, displacement distribution, and time evolution upon excitation with a localized phonon source to illustrate the device behavior and to demonstrate the existence of a phonon Wannier-Stark ladder (WSL) and Bloch oscillations (BO). In addition, using a photoelastic model we calculate the Raman spectra which we show give a direct measure of the created phononic WSL. Phonon BO can be independently probed using coherent phonon generation techniques. For this purpose we propose a specifically designed device and we present calculations of time-dependent reflectivity induced by femtosecond impulsions in this structure.

A periodic stack of two materials with contrasting acoustic impedances reflects sound.[9] The first $k=0$ folded phonon minigap in a SL is maximum with the layers thickness (d) ratio given by $d_1/v_1=d_2/3v_2$, the stop band and reflectivity of such a phonon mirror being determined by the acoustic impedance mismatch $Z=\rho_1 v_1/\rho_2 v_2$ and the number of SL periods.[10,11] A phonon cavity can be constructed by enclosing between two SL's a spacer of thickness $d_c=m\lambda_c/2$, where λ_c is the acoustical phonon wavelength at the center of the phonon minigap.[7] The cavity confined modes correspond to discrete energy states within the phonon stop band, their width (i.e., the cavity Q-factor) being determined by the phonon mirror reflectivity.[10] When a large series of phonon microcavities are coupled one after the other, the discrete confined energy states form phonon bands that resemble the mini-

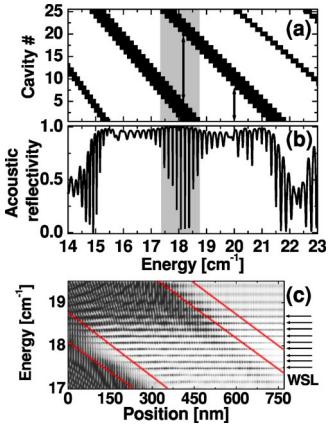

FIG. 1. (a) Phonon band structure. The central white region limited by the thicker black forbidden bands corresponds to the cavity-mode miniband. The white and thinner black regions above and below this bands arise from Bragg reflections. The arrows indicate the energy of the pulses displayed in Fig. 2. (b) Phonon reflectivity. In (a) and (b) shaded areas indicate the WSL region. (c) Phonon displacement as a function of position and energy. Darker regions indicate larger acoustic phonon intensities. The arrows label the WSL energies. The solid lines limit the forbidden bands. See text for details.

bands in electronic SL's. In order to display Bloch oscillations, the energy of the ith cavity must differ from that of the $(i-1)$th in a constant value. Such a linear dependence with position of the phonon cavity-mode energy, analogous to an electric field for electrons, can be obtained by tuning the cavity widths.[4] We thus consider a multilayer structure where each unit cell consists of an acoustic-phonon mirror made by $(n+1/2)$ $\frac{\lambda}{4}/\frac{3\lambda}{4}$ periods of two materials with contrasting acoustic impedances (GaAs/AlAs in the examples discussed here), followed by a λ cavity (GaAs). This unit cell is repeated N_c times with layer thicknesses increasing from the surface to the substrate so as to have a linear decrease of cavity-mode energy by steps of Δ.

The stationary solutions of the acoustic waves in the proposed structure can be derived using a matrix method implementation of the elastic continuum model.[7] The calculations give (i) the phonon field distribution in the different layers, (ii) the phonon reflectivity and/or transmission, and (iii) the variation along the structure of the energy bands associated to an infinite SL with the local unit cell. The latter are given by the condition $-1 \leqslant (a_{11}+a_{22})/2 \leqslant 1$, where a_{11} and a_{22} are the diagonal elements of the transfer matrix across each period of the structure.[4] In Fig. 1 we present results for a $N_c=25$ period acoustic-cavity structure. The first unit cell is made by a 2.5 GaAs/AlAs period 59.3 Å/23.5 Å phonon mirror $(n=2)$ and a GaAs spacer tuned to 20 cm^{-1} (79 Å). The energy steps are given by $\Delta=0.15$ cm^{-1}, and the structure is limited from the two sides by GaAs. Panels (a) to (c) display, respectively, the phonon band structure (black regions represent "forbidden" energies), the phonon reflectivity, and the phonon displacement distribution as a function of position and energy. In the latter panel, calculated for phonons entering from the left, darker regions indicate larger acoustic-phonon intensities. Several features should be highlighted in these figures. (i) An acoustic phonon allowed band originated in the coupled discrete cavity modes is observed between two forbidden minigap bands [panel (a)]. The energy of the bands decreases linearly with cavity number according to design. Three different spectral regions can be identified. Between 17.4 and 18.6 cm^{-1} (shaded in Fig. 1), phonons are confined in a spatial region limited by the top and bottom of the lower and upper minigap bands, respectively. On the other hand, below(above) 17.4(18.6) cm^{-1} a phonon entering from cavity No. 1 will bounce back at the bottom of the lower (upper) minigap band and leave the sample. (ii) The phonon reflectivity [panel (b)] displays a broad stop band (between $\sim$15 and 21.5 cm^{-1}), basically determined by the superposition of the individual cavity minigaps. A series of dips modulate the reflectivity within this wide stop band. Between the lower stop-band limit and $\sim$17.4 cm^{-1}, and between $\sim$18.6 cm^{-1} and the upper stop-band limit, a series of features with varying energy spacing can be identified. These originate from phonon interferences determined by a propagation limited by the sample surface and by the minigap bands. These features are relatively weak and broad because of the small acoustic impedance mismatch between the top GaAs layer and the cavity structure. On the other hand, sharp reflection dips are observed in the region between $\sim$17.4 and 18.6 cm^{-1}. These dips, which are equidistant and separated by $\Delta=0.15$ cm^{-1} correspond to the coupling of external phonons, by tunneling through the minigap band, to the Wannier-Stark states confined within the structure. (iii) This phononic WSL can be also identified by the well-defined discrete phonon modes displayed in panel (c). The WSL is the spectral domain counterpart of the BO. It is precisely in this spectral region where oscillations should appear in the time domain.

The time and spatial variation of the acoustic-phonon displacement field $U_g(z,t)$, created by a pulse described by a spectral function $g(\omega)$ and incident at $t=0$ at the GaAs-sample interface $(z=0)$, can be evaluated using the scattering method described by Malpuech and Kavokin.[4] Within this description, $U_g(z,t)=1/2\pi\int_{-\infty}^{\infty}u(z)g(\omega)\exp(-i\omega t)d\omega$, where $u(z)$ are the stationary solutions of the elastic wave equation with frequency ω shown in Fig. 1(c). The time evolution of such wavepackets for the two different energies indicated in Fig. 1(a) are shown in Fig. 2. For energies above or below the phonon WSL region (20 cm^{-1} in the example shown), the incident pulse propagates within the sample up to a position where it is backreflected by a minigap band leaving afterwards the sample. On the contrary, when ω corresponds to the WSL energy region (18.3 cm^{-1} in the displayed figure), a fraction of the pulse energy is backreflected at the surface while another part enters the structure by tunneling through the minigap band developing afterwards clear periodic oscillations within the structure. In order for these phonon BO to be observed, the full width at half maximum (FWHM) of $g(\omega)$ should be larger than Δ. For these calculations we have used a Gaussian distribution with $2\sigma=1.0$ cm^{-1}. On the other hand, the period of the oscillations (and consequently the length traveled by the pulse) is directly determined by Δ $(\tau_B=h/\Delta)$.

In what follows we will show how Raman scattering and

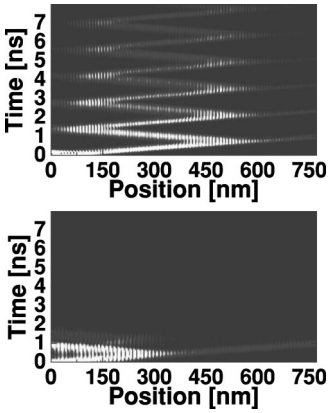

FIG. 2. $\ln(u(z,t))$ for Gaussian phonon wavepackets centered at 20 cm^{-1} (bottom panel) and at 18.3 cm^{-1} (top panel), and FWHM given by $2\sigma=1$ cm^{-1}. These two energies are indicated with arrows in Fig. 1(a).

coherent phonon generation experiments can provide a direct probe of the phonon WSL and BO, respectively, in these devices. Raman scattering has extensively shown to be a powerful tool to study phonons in semiconductor multilayers[11] and, in particular, confined modes in acoustic cavities.[7,10] In order to evaluate the Raman spectra, we use a photoelastic model.[7,11] We analyze two experimental geometries, namely backscattering (BS, $k_S \sim -k_L$, $q=\sim 2k_L$) and forward scattering (FS, $k_S \sim k_L$, $q \sim 0$). Here k refers either to the scattered or laser wavevector, and q is the transferred wave number. In Fig. 3 we present BS and FS spectra calculated for the sample described above and assuming laser excitation with 550 nm. For comparison purposes the corresponding phonon reflectivity is also shown. The Raman spectra display a complex series of peaks in the stop-band spectral region. We have verified that such rich spectra are a kind of sample finger print that can be used as a characterization tool. Interestingly, the BS and FS spectra display clear peaks and dips, respectively, at exactly the WSL energies. High-resolution Raman setups working in the visible can discern spectral features with resolution better than 0.02 cm^{-1},[12] thus providing a spectral-domain tool able to probe the underlying phonon WSL.

Coherent phonon generation is termed the impulsive generation of phonons using high power ultrashort laser pulses.[13] In the case of THz vibrations, femtosecond pulses are required. To the best of our knowledge the generation mechanism is still an open issue, and no complete theory is available to describe the processes involved. We briefly describe next a model for pump and probe coherent phonon generation and detection based on a photoelastic coupling between light and acoustic phonons.[14] This mechanism is the only one active when pump and probe are below the gap. Above the gap besides the photoelastic coupling other mechanisms can also contribute, but we expect the main conclusions to remain essentially valid. Any arbitrary time and position dependent phonon displacement in the structure $w(z,t)$ can be expressed in terms of the phonon eigenstates as $w(z,t)=\int r_\omega u(z)\sin(\omega t)d\omega$. Assuming that phonons are generated coherently through a photoelastic mechanism by a femtosecond pulse [modeled as $E_0(z,t)\propto\delta(t)\exp(ik_L z)$], the coefficients for the above expansion can be obtained as[14] $r_\omega=1/\omega\int_0^L p(z)|E_0(z)|^2[\partial u(z)/\partial z]dz$. Here L is the length of the sample, $p(z)$ is the photoelastic constant which is assumed constant in each layer, and $\partial u(z)/\partial z$ is the strain associated with an eigenstate of energy ω. We note that the FS ($q=0$) Raman cross section discussed above is proportional to $|r_\omega|^2$.[7] Once this excitation is generated, it evolves according to the time-dependence $\sin(\omega t)$ and can be detected by a delayed, lower power, probe pulse that senses the time-dependent change of reflectivity.[15] The change in reflectivity can be calculated as $\Delta R(t)\propto\int_0^\infty \Delta\epsilon(z,t)\exp(2ikz)dz$, where the probe pulse has been assumed to be proportional to e^{ikz}.[15] Introducing again the photoelastic coefficient to relate $\Delta\epsilon$ (the phonon induced change in dielectric function) with the strain $\partial w(z,t)/\partial z$, the time-dependent change in reflectivity can be written as $\Delta R(t)\propto\int_0^\infty p(z)[\partial w(z,t)/\partial z]\exp(2ikz)dz$. If $p(z)$ is constant, this equation implies that only phonons with $q=2k$ can be probed. On the other hand, the detector's $p(z)$ can be designed to access other excitations by backfolding the phonon dispersion. Comparing this equation with the Raman cross section,[7] it is easy to see that the observable phonon spectrum is related to the BS Raman scattering component of the detector structure.

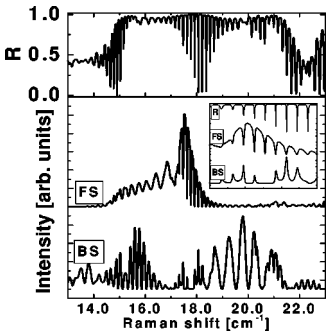

FIG. 3. Back (BS) and forward (FS) 550 nm Raman scattering spectra corresponding to the acoustic cavity structure with $N_c=25$ described in the text. For comparison the corresponding phonon reflectivity is also shown. The inset highlights the Stark ladder spectral region (17–19.5 cm^{-1}).

In order to generate the quasimonoenergetic phonons required to induce BO, and to monitor the time evolution of the latter, we have conceived a monolithic source-sample-detector device (see the scheme in Fig. 4). The first GaAs/AlAs SL (SL/s in Fig. 4) acts as the phonon source and is designed to generate, by excitation with a femtosecond impulsion above the gap, an elastic pulse with energy centered at 18.3 cm^{-1} and width equal to $\sim$0.8 cm^{-1}.[13] It is made of 30 periods of 43.2 Å/51.5 Å GaAs/AlAs. The layer widths determine the energy of the generated pulse, while the number of periods define, due to finite-size effects, its width. The coefficient r_ω of the phonon pulse (or equivalently the FS Raman spectra) generated in this SL is shown in the inset on Fig. 4. Once generated, the coherent phonons propagate into the structure and act as the phonon source $g(\omega)$ for exciting Bloch oscillations. Between the SL source and the structure, a GaAs 200 nm buffer layer is introduced to screen the residual pump power, not absorbed in the SL, from impinging into the cavity structure and generating unwanted

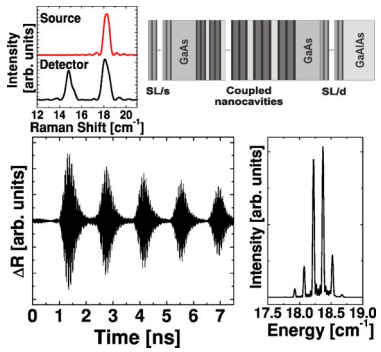

FIG. 4. Top-left, source and detector SL's Raman spectra. Top-right, scheme of the proposed monolithic source-sample-detector phonon device (see text for details). Bottom-left, time variation of the reflectivity probed at the detector SL. Bottom-right, Fourier transform of the detected reflectivity change.

frequencies. The $g(\omega)$ phonon pulse, on the other hand, propagates through the GaAs layer basically unaltered. The cavity structure is identical to the one described above. Once within this structure, Bloch oscillations develop and part of the energy is lost to the substrate upon each turn. Their effect at the right end side of the sample is probed by the second SL (SL/d in Fig. 4), which acts as an energy selective detector of the Bloch oscillations through their effect in the time variation of the reflectivity.[14] To keep this time variation simple, a second GaAs layer is introduced to stop the probe beam from being modulated also by the cavity structure. The BS Raman spectrum of the SL defines the detector's bandwidth, which we have designed to include the pulse $g(\omega)$. It consists of a 20 periods 38.1 Å/68.1 Å GaAs/AlAs SL. Its BS spectrum, calculated for a 750 nm probe pulse, is shown in the inset on Fig. 4. The device is terminated by a thick (>1 μm) $Ga_{0.5}Al_{0.5}As$ layer which acts both as a stop layer for chemically etching the GaAs substrate and as a window for accessing the detector SL from the back. In Fig. 4 we present calculations of the reflectivity change as a function of time. Fast oscillations dominate the reflectivity, corresponding to the frequency of the coherently excited phonons (18.3 cm^{-1}). In addition, this fast component is amplitude modulated by an envelope whose frequency is determined precisely by the Bloch oscillation period. The Fourier transform of the time-dependent reflectivity clearly shows the WSL frequencies within an envelope determined by the input source $g(\omega)$ and the detector bandwidth.

In conclusion we have extended concepts previously discussed in the context of electronic and photonic properties of solids to acoustic-phonon physics. We have described semiconductor structures based in recently reported acoustic cavities and achievable with actual growth technologies, displaying phononic Stark ladders and capable of sustaining Bloch oscillations. We have also shown how Raman scattering and coherent phonon generation provide spectral and time domain probes, respectively, of these acoustic phenomena. Structures as the one described here can be exploited to enhance the coupling between sound and other excitations (electrons and photons), and as the feedback high-Q resonator of a phonon laser. Moreover, engineered phonon potentials are not limited to linear dependencies that mimic electric fields but can take arbitrary shapes. This opens the way to different phonon devices based in the discrete confined states of acoustic cavities.

We acknowledge M. Trigo and B. Perrin for enlightening discussions and G. Malpuech for useful information concerning the porous silicon optical Bloch structures. A.F. also acknowledges support from the ONR (U.S.).

[1] F. Bloch, Z. Phys. **52**, 555 (1928); C. Zener, Proc. R. Soc. London **A145**, 523 (1934).

[2] See, for example J. Feldmann, K. Leo, J. Shah, D. A. B. Miller, J. E. Cunningham, T. Meier, G. von Plessen, A. Schulze, P. Thomas, and S. Schmitt-Rink, Phys. Rev. B **46**, R7252 (1992); C. Waschke, H. G. Roskos, R. Schwedler, K. Leo, H. Kurz, and K. Khler, Phys. Rev. Lett. **70**, 3319 (1993).

[3] S. R. Wilkinson, C. F. Bharucha, K. W. Madison, Qian Niu, and M. G. Raizen, Phys. Rev. Lett. **76**, 4512 (1996).

[4] G. Malpuech and A. Kavokin, Semicond. Sci. Technol. **16**, R1 (2001), and references therein.

[5] R. Sapienza, P. Costantino, D. Wiersma, M. Ghulinyan, C. J. Oton, and L. Pavesi, Phys. Rev. Lett. **91**, 263902 (2003); V. Agarwal, J. A. del Ro, G. Malpuech, M. Zamfirescu, A. Kavokin, D. Coquillat, D. Scalbert, M. Vladimirova, and B. Gil, *ibid.* **92**, 097401 (2004).

[6] G. Monsivais, R. Rodriguez-Ramos, R. Esquivel-Sirvent, and L. Fernandez-Alvarez, Phys. Rev. B **68**, 174109 (2003).

[7] M. Trigo, A. Bruchhausen, A. Fainstein, B. Jusserand, and V. Thierry-Mieg, Phys. Rev. Lett. **89**, 227402 (2002); see also J. M. Worlock and M. L. Roukes, Nature (London) **421**, 802 (2003).

[8] S. I. Tamura, W. Chen, and H. J. Maris, Philos. Mag. B **70**, 3 687 (1994).

[9] V. Narayanamurti, H. L. Störmer, M. A. Chin, A. C. Gossard, and W. Wiegmann, Phys. Rev. Lett. **43**, 2012 (1979).

[10] P. Lacharmoise, A. Fainstein, B. Jusserand, and V. Thierry-Mieg, Appl. Phys. Lett. **84**, 3274 (2004).

[11] B. Jusserand and M. Cardona, in *Light Scattering in Solids V*, edited by M. Cardona and G. Güntherodt (Springer, Heidelberg, 1989), p. 49.

[12] A two meter SOPRA double grating spectrograph can have a resolution around 0.02 cm^{-1}. A tandem Fabry-Perot Raman monochromator setup can improve this perfomance down to 0.005 cm^{-1}. See, e.g., J. P. Pinan, R. Ouillon, P. Ranson, M. Becucci, and S. Califano, J. Chem. Phys. **109**, 5469 (1998).

[13] T. Dekorsy, G. C. Cho, and H. Kurz, in *Light Scattering in Solids VIII*, edited by M. Cardona and G. Güntherodt (Springer, Heidelberg, 2000), p. 169.

[14] M. Trigo, T. Eckhause, and R. Merlin (private communication).

[15] C. Thomsen, H. T. Grahn, H. J. Maris, and J. Tauc, Phys. Rev. B **34**, 4129 (1986).